Elastic scattering of 81-keV γ rays

G. Basavaraju and P. P. Kane

Department of Physics, Indian Institute of Technology, Powai, Bombay 400 076, India

Lynn D. Kissel* and R. H. Pratt

Department of Physics and Astronomy, University of Pittsburgh, Pittsburgh, Pennsylvania 15260

(Received 31 August 1993)

A high-purity germanium detector was used to determine differential cross sections for the elastic scattering of 81-keV γ rays by aluminum, nickel, tantalum, gold, and lead through angles of 60°, 90°, 120°, and 133°. The atomic Rayleigh scattering amplitudes were obtained in the independent-particle approximation by calculations of modified relativistic form factors (MF's), a combination of MF's and angle-independent "anomalous" scattering factors (ASF's), and the relativistic second-order S matrix. Most experimental cross sections for gold and lead are slightly smaller than the calculations in the S matrix or the MF-ASF approaches, the differences being larger in the latter case. The calculated cross sections based on MF's are enormously larger than these values. The tantalum data are in good agreement with S-matrix calculations. The data for Al show agreement with the different calculations, which differ by less than about 6%.

PACS number(s): 32.80.Cy

I. INTRODUCTION

Elastic scattering of γ rays and hard x rays by bound atomic electrons is usually called Rayleigh scattering. The form-factor approximation (FFA) has been found to be useful for the description of Rayleigh scattering, especially for small-momentum transfers and photon energies much larger than K-shell electron binding energies. Significant deviations from the predictions of FFA's are expected in general when the stated conditions are not applicable, and in particular when photon energies are close to electron binding-energy thresholds. Several studies of γ-ray scattering performed with semiconductor detectors (e.g., [1–13]) have confirmed the above-mentioned expectations. Gamma rays of 88.03, 84.3, and 81.0 keV were used in the first four studies, the remaining studies having been done with 59.54-keV γ rays. Since relativistic effects are more important with increasing atomic number Z, there is an increasing interest in pursuing such investigations in the photon energy range covering K-shell thresholds of stable elements of very high Z, i.e., from about 80 to 90 keV. The departures from form factors are expressed in terms of energy-dependent, complex "anomalous" scattering factors (ASF's), which have been usually assumed to be independent of angle [14]. Alternatively in some cases, elaborate calculations based on the relativistic second-order S-matrix treatment have been carried out (e.g., [15,16]).

In order to provide an extensive test of current theoretical understanding, measurements were performed with targets of aluminum, nickel, tantalum, gold, and lead at

*Permanent address: Computational Physics Group L-59, Lawrence Livermore National Laboratory, Livermore, CA 94550.

angles between 60° and 133°. Calculations of modified relativistic form factors (MF's), anomalous scattering factors, and S-matrix elements were carried out and are described in Sec. II. Details regarding the experimental procedures are outlined in Sec. III. In Sec. IV, conclusions are presented on the basis of comparisons of experimental data with theoretical calculations.

II. THEORETICAL CALCULATIONS

In the case of 81-keV γ rays, Delbrück scattering amplitudes are negligible and nuclear scattering is well represented by the nuclear Thomson scattering amplitude $r_0 f_T$, where $r_0 = e^2/mc^2$, $f_T = Z^2(m/Am_p)$, e is the electron charge, c is the speed of light, m and m_p are electron and proton masses, respectively, A is the atomic weight, and Ze is the nuclear charge. In nonrelativistic theory, Rayleigh scattering arises through the photon-electron interaction Hamiltonian terms $e^2 \mathbf{A} \cdot \mathbf{A}/(2mc^2)$ and $(-e\mathbf{p} \cdot \mathbf{A}/mc)$, where $\mathbf{A}$ is the vector potential of the radiation and $\mathbf{p}$ is the electron momentum operator. In the cases studied in the present experiment, the nuclear Thomson scattering amplitude, though not entirely negligible, is less than 2% of the corresponding Rayleigh amplitude. The A^2-dependent term alone leads to the form-factor description of atomic Rayleigh scattering cross section $d\sigma_R/d\Omega$, and to Eq. (1) in the case of unpolarized incident photons:

$$\frac{d\sigma_R}{d\Omega} = \tfrac{1}{2}r_0^2(1+\cos^2\theta)|f(q)|^2 , \qquad (1)$$

where

$$f(q) = 4\pi \int_0^\infty \frac{\rho(r)\sin(qr)r^2 dr}{qr} , \qquad (2)$$

$$\hbar q = 2(\hbar\omega/c)\sin(\theta/2) , \qquad (3)$$

where $\hbar q$ is the momentum transfer in scattering, $\hbar = h/2\pi$, h is Planck's constant, ω is the angular frequency of the radiation, θ is the scattering angle, and $\rho(r)$ is the electron number density at a distance r from the center of an atom. Note that the elastic scattering cross section is obtained by the coherent addition of the nuclear Thomson and the Rayleigh contributions, e.g., in the FFA by the replacement in Eq. (1) of $f(q)$ by $[f(q)+f_T]$.

When electron binding correction is introduced, the corrected form factor $g_i(q)$ for the ith subshell with the corresponding density $\rho_i(r)$ calculated relativistically is known as the modified relativistic form factor (MF). If E_i and ε_i are respectively the total energy and binding energy of an electron in the ith subshell, $E_i = (mc^2 - \varepsilon_i)$, and $V(r)$ is the potential energy at a distance r from an atomic center, we obtain Eq. (4):

$$g_i(q) = 4\pi \int_0^\infty \frac{\rho_i(r)\sin(qr)r^2}{qr} \frac{mc^2}{[E_i - V(r)]} dr \ . \qquad (4)$$

The total atomic $g(q)$ is the sum of $g_i(q)$ over occupied subshells. In comparison with the simple form-factor approach, the use of modified form factors incorporating binding corrections at least partially in an approximate way is expected and indeed found to provide a better representation of many experimental data. Of course, additional considerations are needed under the circumstances mentioned in Sec. I.

The p·A interaction term leads to the introduction of explicitly energy-dependent real and imaginary anomalous scattering factors f' and f'' or g' and g'', in the two schemes respectively. Accordingly, in Eq. (1) for the atomic Rayleigh scattering cross section, $|f(q)|^2$ will be replaced by $[|f(q)+f'|^2 + |f''|^2]$, or by $[|g(q)+g'|^2 + |g''|^2]$, respectively. From the optical theorem, it is known that the dominant part of the anomalous scattering factor f'' or g'' in the forward direction is proportional to the photoeffect cross section at the same energy. A dispersion relation connecting the real and imaginary parts of the Rayleigh amplitudes is then used to calculate the real part of ASF's.[16] Since a method for the calculation of angular variations of ASF's is not yet available, ASF's are frequently assumed to be independent of angle.

In a previous work [14], it was demonstrated that the real anomalous scattering factors $f'(\omega)$ calculated by Cromer and Liberman [17,18] rely on the dipole approximation in obtaining the high-energy limit $f'_{CL}(\infty)$, even though that approximation is not correct at high energies. Then a correction term $\delta f'$ is needed to obtain $f'(\omega)$:

$$f'(\omega) = f'_{CL}(\omega) + \delta f' \qquad (5)$$

and

$$\delta f' = f'(\infty) - f'_{CL}(\infty) \ , \qquad (6)$$

where $f'(\infty)$ is the correct high-energy limit of f'. Note that $g''(\omega) = f''(\omega)$ and $g'(\omega)$ is given by Eq. (7), since the modified form factor $g(q)$ accounts correctly for the high-energy limit of the Rayleigh amplitude:

$$g'(\omega) = f'_{CL}(\omega) - f'_{CL}(\infty) \ . \qquad (7)$$

As shown earlier [14], the correction term changes the calculated cross section by as much as 40% in the case of 59.54-keV photon scattering by lead through 180°. Further, the same type of correction also removes to a large extent the deviations noticed between accurate experimental values of f' for silicon up to about 45 keV [19] and Cromer-Liberman calculations.

Relativistic MF and ASF calculations have now been performed for 81.000-keV γ rays on the basis of a potential incorporating a local Slater exchange and a Latter tail. The contributions of bound-to-bound transitions have been included in the evaluation of ASF's. Note that the experimentally determined binding energy ε_K of a gold K-shell electron is 0.277 keV below 81 keV, but that the calculated value of ε_K according to the Dirac-Slater model is 81.007 keV. Thus an energy-shifting procedure was adopted in the case of calculations for gold. The photon energy was varied upwards from 81.007 keV in steps of 0.05 eV to 81.017 keV, then in steps of 1 eV up to 81.027 keV and in larger steps above 81.027 keV. In the energy range between about 81.2 and 81.4 keV, i.e., for a photon energy excess above 81.007 keV of more than 0.2 keV and less than 0.4 keV, the calculated cross sections differed by less than a few percent and thus are not very sensitive to the assumed value of photon energy excess.

Relativistic second-order S-matrix calculations were carried out in the cases of relatively strongly bound or "inner" subshells for which the ratio of photon energy to the subshell binding energy was less than 300. This condition is satisfied in the case of tantalum for example by K, L, M, and N_1 to N_3 subshells. In the case of gold and lead, N_4 and N_5 subshells also satisfy this condition. The calculations for "outer" electrons were carried out by the simpler procedure described in detail earlier [16]. As in the case of ASF calculations, an energy-shifting procedure was necessary for the evaluation of cross sections for gold. In the S-matrix calculations, the cross sections differed by less than 1.5% for angles larger than 60° as long as the chosen photon energy excess was within ±15 eV of the expected value of 277 eV. A test was also made of the sensitivity of the calculations to the nature of the assumed exchange potential. If the Kohn-Sham ($\frac{2}{3}$ Slater) exchange potential is used, the calculated value of ε_K in the case of gold is 80.591 keV. For a photon energy excess within ±15 eV around the expected value of 277 eV, the cross sections calculated with the Kohn-Sham exchange differed from those calculated with the Slater exchange by less than about 1.5%.

The calculated values of cross sections are presented in tabular and graphical forms in Sec. IV.

III. EXPERIMENTAL DETAILS

A thin ^{133}Ba source of strength 7.4×10^8 Becquerel (~ 20 m Ci) and 0.1-cm diameter was used to provide 81-keV γ rays. The source also emits a stronger intensity of 356-keV γ rays and weaker intensities of γ rays of 53.2, 79.6, 160.6, 223.1, 276.4, 302.8, and 383 keV [20]. The source was housed at the center of a cylindrical lead

shield of 15.5-cm diameter and 18-cm length. The lead shield was covered with brass of 0.6-cm thickness in order to attenuate K x rays of lead. The γ rays from the source emerged through a brass-lined collimator of 0.8-cm diameter and 10-cm length. The entire source housing was mounted on an arm which could be rotated about a vertical direction passing through the target center. The distance between the source and the target center was 23 cm.

Targets of better than 99.5% purity were mounted in conventional reflection geometry with thin tapes on light frames which were well outside the spread of the γ-ray beam. The targets were thin enough to ensure an effective transmission for elastically scattered 81-keV γ rays larger than 0.66. The normal target thicknesses were 0.900, 0.360, 0.0249, 0.0252, and 0.0939 g/cm^2, respectively, in the case of aluminum, nickel, tantalum, gold, and lead. In order to determine the contribution of possible secondary effects such as multiple scattering, thinner targets of 0.121-g/cm^2 aluminum and 0.180-g/cm^2 nickel, and thicker targets of 1.800-g/cm^2 aluminum and 0.0905-g/cm^2 gold, were also utilized.

The distance from the target to the center of the planar high-purity germanium detector was 23 cm. The detector supplied by EG&G ORTEC had a diameter of 1.6 cm and a thickness of 1.0 cm. The preamplifier output was connected to a Tennelec TC 242 amplifier whose output was analyzed by an IBM personal-computer- (PC-) based 4096-channel pulse-height analyser supplied by Nucleonix Ltd., Hyderabad, India. The system FWHM (full width at half maximum) at 81 keV was about 0.46 keV, and was therefore adequate to resolve the photopeaks of 81- and 79.6-keV γ rays from the source. Two different cylindrically symmetric shielding arrangements employing brass-lined lead or tungsten carbide were used close to the detector. The opening in front of the detector had a diameter of 5 cm in the case of lead shielding, and 2 cm in the case of tungsten carbide shielding. Both the shields had lengths of 12 cm and outer diameters of 11 cm. Of course, as expected, the background counts determined in the absence of any target were lower with the tighter shield. But the net target-dependent counts were found to be independent of the differences between these two shielding arrangements.

As described previously [1], the error in the measured elastic-scattering cross section $d\sigma_{el}/d\Omega$ is reduced if the elastic-scattering counts due to a target under study are compared with the Compton scattering counts N^{Al}_{Comp} due to an aluminum target. With such a procedure, the source strength and the detector solid angle do not need to be determined, and only ratios of quantities such as detection efficiencies and target transmissions for similar energies are needed. Then we have

$$\frac{N_{el}}{N^{Al}_{Comp}} = \frac{M^t}{M^{Al}} \frac{A^{Al}}{A^t} \frac{T_{81}}{T^{Al}_{Comp}} \frac{\epsilon_{81}}{\epsilon_{Comp}} [d\sigma^{Al}_{Comp}/d\Omega]^{-1} \frac{d\sigma_{el}}{d\Omega} ,$$

$$(8)$$

where M^t and M^{Al} are the masses per unit area of the target under study and of aluminum, respectively, A^t and A^{Al} are the atomic weights of the target under study and

of aluminum, T_{81} and T^{Al}_{Comp} are the transmissions for 81-keV elastic scattering with the target and for corresponding Compton scattering with aluminum, ϵ_{81} and ϵ_{Comp} are the photopeak detection efficiencies for 81 keV and for the energy after Compton scattering, and $d\sigma^{Al}_{Comp}/d\Omega$ is the Compton scattering cross section of an aluminum atom for 81-keV γ rays. The last-mentioned cross section is calculated reliably through the incoherent scattering function approach [21], since the binding energies of electrons in a low-Z atom are very small in comparison with 81 keV:

$$\frac{d\sigma^{Al}_{Comp}}{d\Omega} = \frac{d\sigma^{KN}}{d\Omega} S(x, Z = 13) ,$$

$$(9)$$

where $d\sigma^{KN}/d\Omega$ is the differential cross section for Compton scattering by an electron according to the well-known Klein-Nishina formula, $S(x, Z = 13)$ is the incoherent scattering function for aluminum, and x is given by Eq. (10):

$$x = \sin(\theta/2)/[\lambda \, (\text{Å})] ,$$

$$(10)$$

where θ is the angle of scattering and λ is the wavelength of the incident radiation in Å.

Pulses arising from the detection of γ rays of energies higher than 81 keV give rise to a continuum underlying the photopeaks due to elastic scattering and Compton scattering of 81-keV γ rays. Uncertainties in the estimation of the continuum intensities contribute to errors in the experimental determination of cross sections.

Scattered beam spectra obtained in one set of measurements at 133° are shown in Fig. 1 for tantalum in the neighborhood of 81 keV, and in Fig. 2 for aluminum near
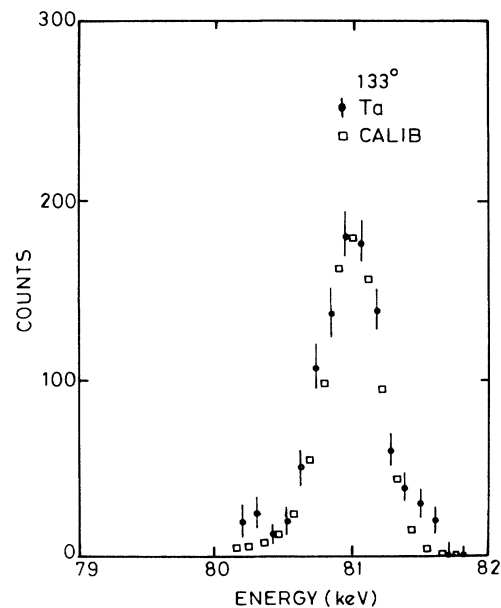

FIG. 1. Net counts obtained with the tantalum target in 30 h at 133°, in the neighborhood of the pulse height corresponding to 81 keV. The shape of the calibration source spectrum determined in 2000 s is represented by squares, the statistical errors being smaller than the sizes of the squares.
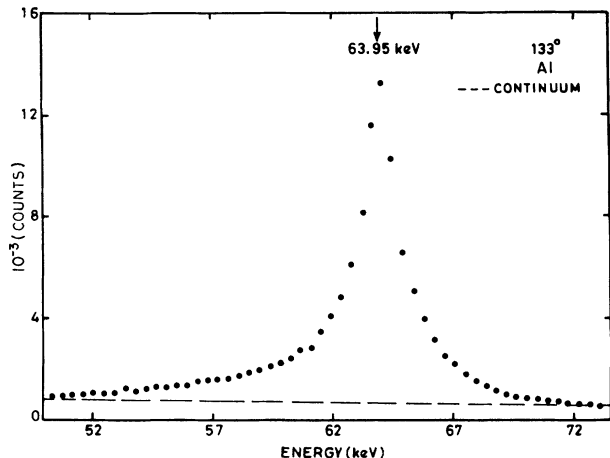
FIG. 2. Net counts obtained with the aluminum target in 64 h at 133°, in the neighborhood of the Compton peak. In order to avoid crowding of data points, only fourth consecutive points are shown. The statistical errors are smaller than the sizes of the points. As indicated by the arrow, the peak of 81-keV γ rays after Compton scattering is at 63.950 keV. A continuum due to higher-energy γ rays is shown by the dashed line. See Sec. III for further details.

FIG. 3. Net counts obtained with the aluminum target in 16 h at 60°, in the neighborhood of the pulse height corresponding to 81 keV.

the Compton peak. For comparison purposes, the squares in Fig. 1 show a thin calibration source spectrum recorded in 2000 s and scaled down by a factor of about 0.01. The statistical errors of the calibration source data are smaller than the sizes of the squares. The full width at half maximum of the elastic scattering peak in Fig. 1 is about 0.54 keV, and is slightly larger than that of the calibration spectrum on account of unavoidable pulse height shifts during the long scattering run. Note that the width of the Compton spectrum is expected to be much larger than that of the elastic-scattering peak on account of the finite angular acceptance, $\sim \pm 2°$ in this experiment, and the momentum distribution of electrons in the scatterer [22,23]. It is seen to be ≤ 1.8 keV in Fig. 2. Therefore, the Compton peak around 63.07 keV arising from the weak ($\sim 8.14\%$) intensity of 79.6-keV γ rays (see Ref. [20]) cannot be resolved from the Compton peak of 81-keV γ rays around 63.95 keV. But a resulting asymmetry on the low-energy side of the peak is observable. If data on the high-energy side of the peak are then analyzed in terms of a Compton profile according to the impulse approximation [22,23], a p_z value of about 0.008 mc is obtained corresponding to the half-intensity point and is quite consistent with that obtained from 59.54-keV scattering data presented in Fig. 3 of Ref. [23]. Here, p_z is the component of initial-state electron momentum along a direction parallel to the scattering vector. The intensities of the two unresolved Compton peaks are proportional to the products of the respective source emission probabilities; T^{Al}_{Comp}, ϵ_{Comp}, and $d\sigma^{Al}_{Comp}/d\Omega$. The three aforementioned factors vary slowly with decreasing photon energy, and in a partially compensating manner. Thus at 133°, the 79.6-keV contribution to the composite Compton peak was estimated to be 8.2% of that of 81-keV γ rays, and was allowed for in the determination of
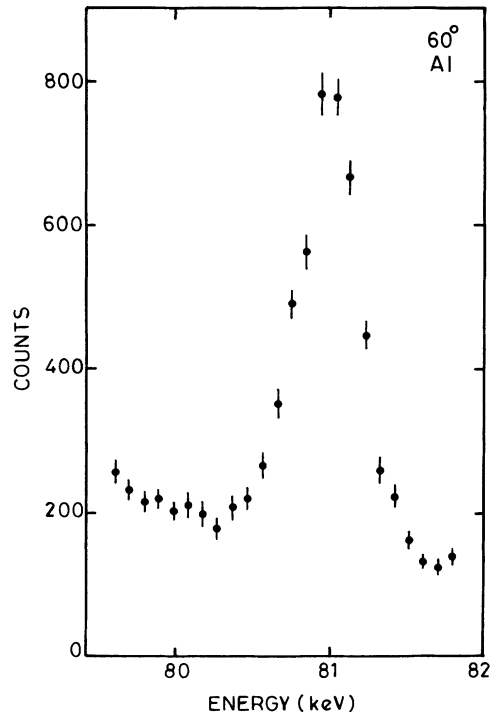
the 81-keV Compton intensity. In the latter case, the statistical error was less than 1%, but the combined error on account of the previously mentioned features was about ±5%.

Net counts N_{el} due to elastic scattering of 81-keV γ rays varied from about 20 per hour in the case of aluminum at 133°, to about 250 per hour in the case of lead at 60°. The background counts in the absence of a target varied from 20–30 per hour. Several sets of measurements were made at each angle, sometimes also with different amplifier gains, and counting times of about 40 h were used with each target at each angle. The errors in N_{el} were about ±10% in the case of aluminum, and between ±4% and ±9% in the case of the other targets.

The target masses were measured with an analytical balance to an accuracy of ±2 mg. The transmission factors were calculated with the help of attenuation coefficients interpolated between the values tabulated by Storm and Israel [24]. With the thin targets in reflection geometry, a possible error of 5% in attenuation coefficients leads to less than 1.5% error in the values of T factors. As shown previously [1], the germanium detector efficiencies between 56.3 and 88 keV could be determined from the measurements of relative intensities of $K\alpha_2$, $K\alpha_1$, $K\beta_1'$, and $K\beta_2'$ x rays of tantalum, gold, and lead. The deduced values of the ratio $\epsilon_{81}/\epsilon_{Comp}$ varied from 0.95 at 60° to 0.85 at 133°, with an estimated error of ±3%. Note that these values are consistent with those determined by an alternative method which relies on measurements of intensities of different γ rays from a thin ^{133}Ba source, and attenuation coefficients and

BASAVARAJU, KANE, KISSEL, AND PRATT

photoeffect to Compton ratios for germanium from a recent tabulation [25].

The errors arising from the different ratios in Eq. (8) were combined in quadrature in order to determine the errors in $d\sigma_{el}/d\Omega$.

Additional representative data for net counts in the neighborhood of 81 keV obtained at 60° with aluminum and lead are presented in Figs. 3 and 4, respectively. The counts shown in the figures below about 80.3 keV arise clearly from the previously mentioned continuum and the elastic scattering of 79.6-keV γ rays.

The data obtained in the case of gold at 133° are shown in Fig. 5. A broad and relatively intense peak is observed in the neighborhood of 80.3 keV, with a slight shoulder near 81 keV. These features of the distribution arise from unresolved peaks due to gold $K\beta_2'$ x-ray components at 80.078, 80.177, 80.380, 80.660, and 80.720 keV, and elastically scattered γ rays of 79.6 and 81 keV. Although the absolute transition probabilities for the different $K\beta_2'$ x-ray components are different according to different atomic models, e.g., the Dirac-Slater model [26] or the Dirac-Fock model [27], the ratios of the transition probabilities turn out to be nearly the same in the two models. A least-squares-fitting routine employing seven Gaussians with a common but adjustable width and the previously mentioned known ratios was utilized to separate gold data over a range of about 2.2 keV into the seven constituent contributions. The combined spectrum resulting from the best fit is also shown in Fig. 5, for convenience of presentation, by a smooth curve. The generally good
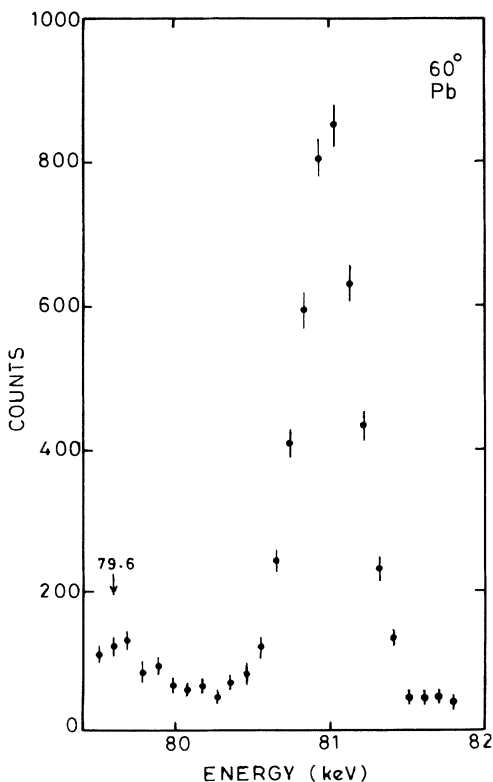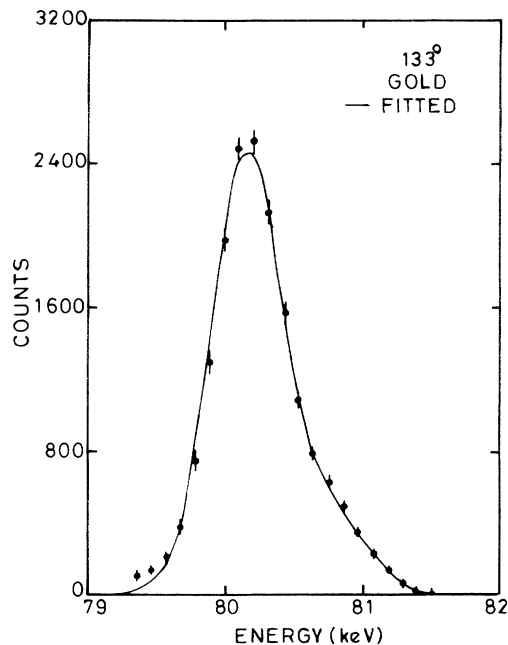

FIG. 5. Net counts arising from gold $K\beta_2'$ x rays, and elastically scattered 79.6- and 81-keV γ rays obtained with the gold target in 51 h at 133°. The spectrum calculated by a least-squares-fitting procedure is represented by the solid curve. See Sec. III for details.

fit is somewhat poor in the two lowest channels because of the higher channel tail of the more intense $K\beta_1'$ x rays at slightly lower energies. The separation of the fitted total spectrum into seven constituent peaks is shown in Fig. 6. Here a logarithmic scale has been used, since the intensity of the weakest component near 80.72 keV is only about 0.003 of that of the strongest component at 80.177 keV. Note that 81-keV elastic scattering contributes only about 12% of the total counts in an interval of 1.2 keV centered at the channel corresponding to 81 keV. A quantitative idea of the goodness of the fit in Fig. 5 can be obtained by the following procedure. Let C_{ex}^i and C_f^i, respectively, represent the measured and fitted counts in ith channel. If the error in C_{ex}^i is E^i, then $\chi^i = (C_{ex}^i - C_f^i)/E^i$ and χ^2 per degree of freedom is defined as the sum of $(\chi^i)^2$ divided by $(n-p)$, where n is the number of data and p is the number of adjustable parameters in the fitting procedure. For the data shown in Fig. 5, χ^2 was 1.18. Good fits were also obtained at 60°, 90°, and 120°, the corresponding χ^2 values being 0.84, 0.66, and 0.83, respectively. Since the 81-keV elastic-scattering peak was not resolved from the gold $K\beta_2'$ x-ray peaks, the errors in the gold cross sections are larger than those in the other cases.

As an independent check of the above-mentioned procedure, an additional experiment was performed with 88.03-keV γ rays of a [109]Cd source exciting the gold K x rays. In this case, the 80–81-keV range included only the five components of gold $K\beta_2'$ x rays. The good fit of experimental data with the resultant of the five components is shown in Fig. 7. Note that in this case the fit is also

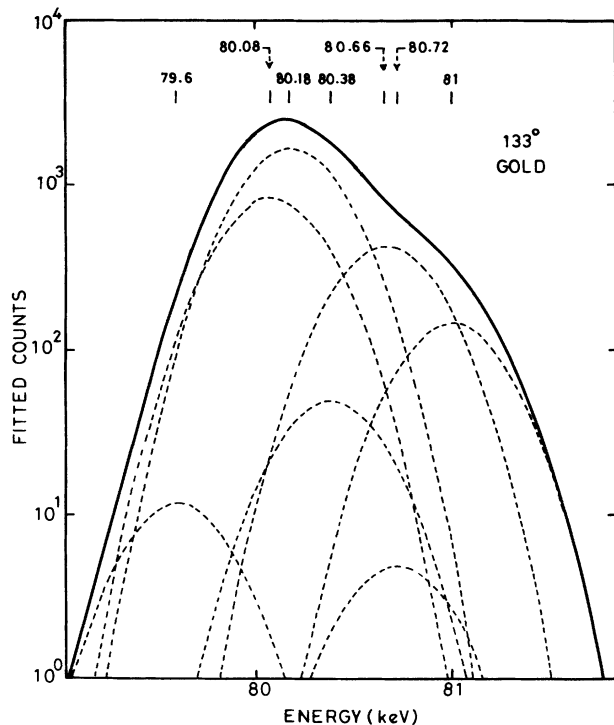FIG. 4. Same as for Fig. 3, except that a lead target was used instead of aluminum.

FIG. 6. The fitted spectrum in Fig. 5 is shown on a logarithmic scale along with the seven constituent Gaussians representing five gold $K\beta_2'$ x-ray components, and elastically scattered 79.6- and 81-keV γ rays.
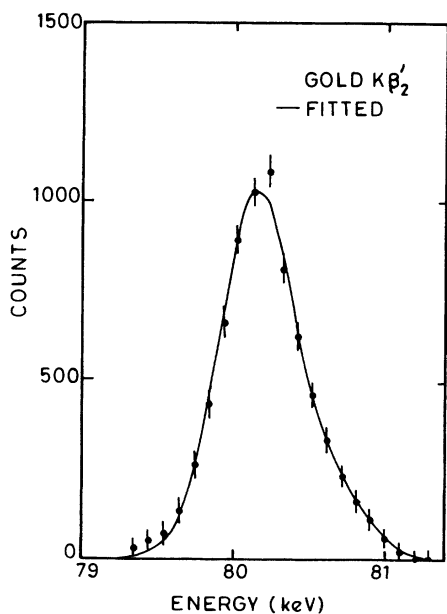

FIG. 7. Spectrum obtained in 20 h from only gold $K\beta_2'$ x rays excited by 88.03-keV γ rays from a [109]Cd source. The solid curve shows the spectrum calculated by a least-squares-fitting procedure employing only five Gaussians in this case to represent the gold $K\beta_2'$ x-ray components.

somewhat poor in the two lowest channels shown, on account of the tail of $K\beta_1'$ x rays.

The final experimental results for 81-keV elastic-scattering cross sections are presented in Sec. IV.

IV. RESULTS AND CONCLUSIONS

The main focus of the present study is on angular distributions of γ-ray elastic-scattering cross sections near K-shell thresholds ε_K of stable elements of very high Z. Note that the γ-ray energy of 81 keV is about 7 keV below ε_K of lead. In previous measurements at six angles between 60° and 150° [5], the 59.54-keV photon energy was about 7.9 keV below ε_K of tantalum. Therefore, qualitative similarities are expected between the results in these two cases, and are indeed observed. Further since the experimental value of ε_K in the case of gold is 80.723 keV, "anomalous" scattering effects have been probed in the present study at an energy much closer to ε_K than in most other studies [2,3,5–13] mentioned in Sec. I. The measured cross sections are not expected to be appreciably influenced by solid-state environment effects in the range from 3.266 to 5.991 of the momentum-transfer parameter x for this experiment. Thus the experimental results have been compared with calculations for isolated atoms. In the case of aluminum ($Z = 13$) with ε_K as low as 1.56 keV, the cross sections, including the effect of nu-
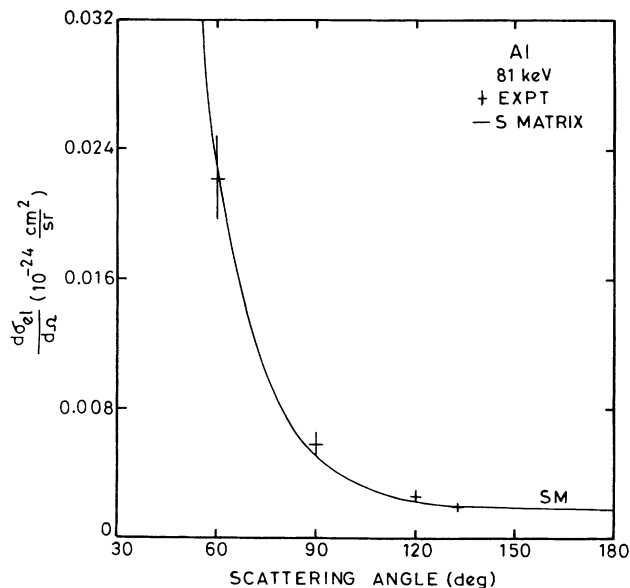

FIG. 8. Differential cross sections for elastic scattering of 81-keV γ rays by aluminum. The theoretical values are obtained by the coherent addition of nuclear Thomson and atomic Rayleigh amplitudes. The latter are calculated with relativistic modified form factors (MF's), with combinations of MF and "anomalous" scattering factors (ASF's), and with the relativistic second-order S-matrix treatment. See Sec. II for details, and Sec. IV for conclusions. Note that cross sections calculated according to MF and MF-ASF schemes in the case of aluminum are not very different from the corresponding values obtained by the S-matrix treatment and are therefore not shown separately in this case.

BASAVARAJU, KANE, KISSEL, AND PRATT

clear Thomson scattering, calculated on the basis of modified form factors (MF's), combinations of MF and anomalous scattering factors (ASF's), and the relativistic second-order S matrix differ by less than about 6% in the relevant cases (Table I). The experimental results for aluminum presented in Table I and Fig. 8 are in good agreement with these calculations.

The experimental and theoretical results for nickel, tantalum, gold, and lead are listed in Table I, and are also presented graphically in Figs. 9, 10, 11, and 12, respectively.

In the case of nickel ($Z = 28$, $\varepsilon_K = 8.333$ keV), the angle-independent real anomalous term $g'(= +0.0835)$ is of the order of 5–10% of $g(q)$, and $|g''|^2$ is less than 0.5% of $|g(q)|^2$. In Fig. 9 for nickel, the experimental values with 8–10% errors do not show a consistent trend

over the whole angular range with respect to any one of the three methods of calculation. However, it can also be seen from the caption of Table I that for nickel the average value 3.29 of χ^2 with the MF-ASF approacah is significantly larger than 2.26 with the MF calculation or 2.10 with the S-matrix treatment.

Experimental values with about 10% errors in the case of tantalum ($Z = 73$, $\varepsilon_K = 67.4$ keV) show excellent agreement with S-matrix calculations. In this case, the modified form factor $g(q)$ decreases from about 6.99 at 60° to 3.41 at 133°, and the angle-independent real anomalous term g' is -0.359. Over this angular range, $g'/g(q)$ varies from about -0.05 to -0.1, and $|g''|^2/|g(q)|^2$ increases from 0.12 to 0.51. So the cross sections calculated in the MF-ASF approach are only moderately larger than the MF results, the differences be-

TABLE I. Cross sections for the elastic scattering of 81-keV γ rays. The theoretical values are calculated by the coherent addition of nuclear Thomson and atomic Rayleigh scattering contributions. The latter have been obtained on the basis of relativistic modified form factors (MF's), a combination of MF and anomalous scattering factors (MF-ASF), and also the relativistic second-order S matrix. The calculated values of cross sections are given in columns 2, 3, and 4, respectively. The experimental cross sections σ_{expt} along with errors Δ appear in column 5. If σ_S is the calculated value in column 4, $\chi_S = (\sigma_{\text{expt}} - \sigma_S)/\Delta$ and $(\chi_S)^2$ is listed in the last column. For Al, Ni, Ta, Au, and Pb, average values of $(\chi_S)^2$ are, respectively, 0.60, 2.10, 0.06, 1.17, and 2.13; average values of similarly defined $(\chi_{\text{MF-ASF}})^2$ are 0.59, 3.29, 1.00, 1.29, and 7.06; and average values of similarly defined $(\chi_{\text{MF}})^2$ are 0.85, 2.26, and 0.70 in the case of Al, Ni, and Ta, respectively. In the case of Au and Pb, σ_{MF} is larger than 1.4 times σ_{expt} and so χ_{MF} is not listed. All cross sections are given in 10^{-24} cm^2/sr. See Sec. II for more details regarding calculations.

| θ (deg) | Calculated cross section (b/sr) | | | σ_{expt} (b/sr) | $(\chi_S)^2$ |
	MF	MF-ASF	S matrix		
Al					
60	0.023 66	0.024 07	0.023 82	0.022 2±0.002 6	0.38
90	0.004 928	0.005 094	0.005 043	0.005 82±0.000 70	1.24
120	0.002 247	0.002 374	0.002 353	0.002 63±0.000 33	0.72
133	0.001 929	0.002 057	0.002 033	0.001 96±0.000 30	0.05
Ni					
60	0.132 8	0.146 8	0.141 3	0.125±0.011	2.11
90	0.049 28	0.057 08	0.054 39	0.0570±0.0043	0.37
120	0.041 98	0.050 11	0.047 73	0.0505±0.0040	0.49
133	0.043 40	0.052 39	0.049 50	0.0397±0.0042	5.44
Ta					
60	2.435	2.486	2.377	2.35±0.20	0.02
90	0.7935	0.9070	0.8467	0.843±0.096	0.00
120	0.6639	0.8348	0.7693	0.741±0.082	0.12
133	0.6831	0.8931	0.8082	0.783±0.083	0.09
Au					
60	3.268	1.429	1.531	1.26±0.19	2.02
90	0.9449	0.4444	0.4356	0.386±0.058	0.74
120	0.7779	0.4967	0.4415	0.549±0.082	1.70
133	0.8138	0.5803	0.4931	0.461±0.069	0.22
Pb					
60	3.790	2.709	2.552	2.21±0.17	4.00
90	1.059	0.5888	0.5354	0.518±0.045	0.14
120	0.8423	0.3992	0.3572	0.314±0.033	1.70
133	0.8843	0.4006	0.3526	0.304±0.030	2.67
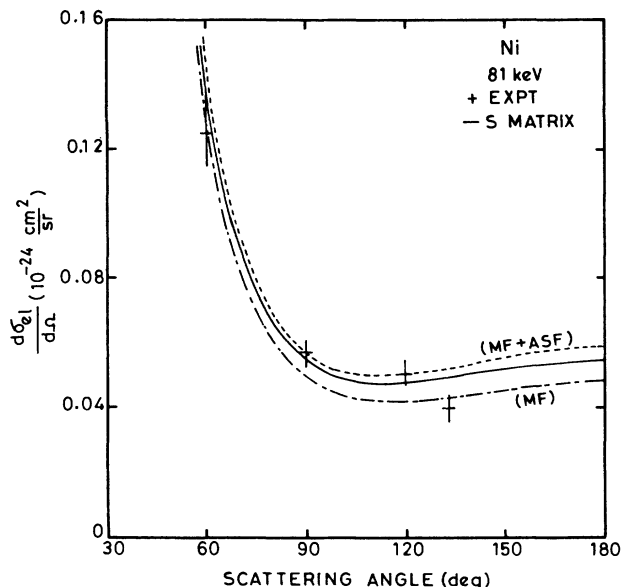
FIG. 9. Same as for Fig. 8, except that nickel is the scatterer.

FIG. 11. Same as for Fig. 8, except that gold is the scatterer.

tween them increasing from about 2% at 60° to 30% at 133°. The tantalum data in Table I are in fair agreement with either the MF or MF-ASF calculations, and in Fig. 10 are seen to be approximately midway between the two calculations for $\theta \geq 90°$.

An idea of the nature of variation of ASF's with photon energy near ε_K can be obtained from previously published interferometric and theoretical work, respectively [28,29]. The MF cross sections are nearly three times larger than the experimental values for gold at 60°, and for lead at 133°. This trend can be understood since, corresponding to these two cases, g' and $g(q)$ are -3.776 and 8.097, and -1.391 and 3.881, respectively. In this

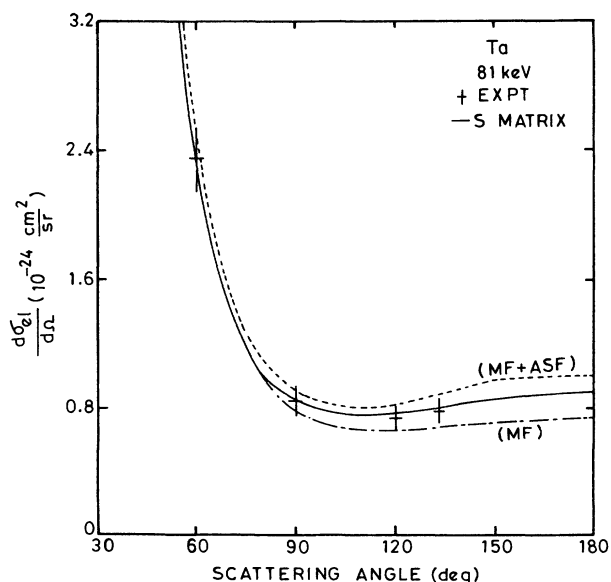context note also that $|g''|^2$ is 9.973 for gold but only 0.5952 for lead. The MF-ASF calculations follow the trend of the experimental data for gold except near 133°, but are systematically somewhat larger than experimental values in the case of lead. As mentioned in the beginning of this section, the MF-ASF calculations for tantalum with 59.54-keV γ rays are also similarly larger than the corresponding experimental values obtained previously [5]. In Figs. 11 and 12, the experimental results show reasonable agreement with S-matrix calculations.

It is evident from Table I that the cross sections calculated according to the MF-ASF scheme have turned out to be systematically a little larger than the S-matrix results, except for gold at 60°. The probable reasons for the

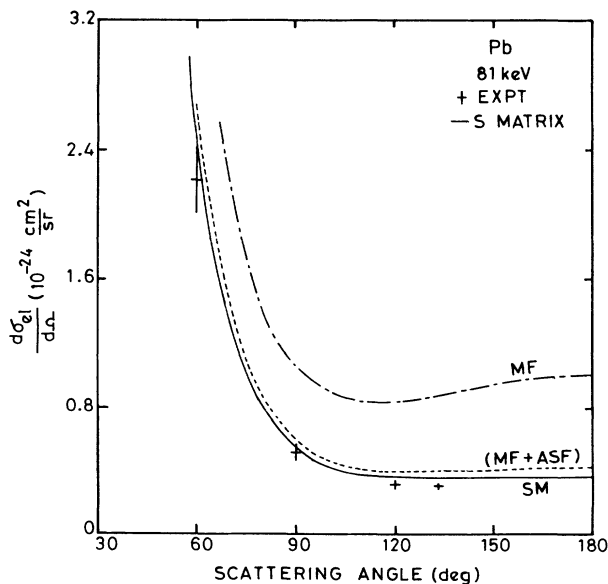FIG. 10. Same as for Fig. 8, except that tantalum is the scatterer.

FIG. 12. Same as for Fig. 8, except that lead is the scatterer.

differences need to be studied in detail, since the simpler MF-ASF approach has to be used in many cases (e.g., [30]) due to a lack of availability of elaborate S-matrix calculations.

[1] P. P. Kane, G. Basavaraju, S. M. Lad, K. M. Varier, L. Kissel, and R. H. Pratt, Phys. Rev. A **36**, 5626 (1987).

[2] G. K. Raju, M. S. Prasad, K. Venkataramanaiah, K. Narasimhamurty, and V. A. Narasimhamurty, Ind. J. Phys. A **62**, 190 (1988).

[3] K. Siddappa, N. G. Nayak, K. M. Balakrishna, N. Lingappa, and Shivaramu, Phys. Rev. A **39**, 5106 (1989).

[4] G. Basavaraju, P. P. Kane, L. Kissel, and R. H. Pratt, in *X-93 International Conference Abstracts, Debrecen, Hungary*, edited by L. Sarkadi and D. Berényi (Institute of Nuclear Research of the Hungarian Academy of Sciences, Debrecen, 1993), p. 64.

[5] M. Schumacher and A. Stoffregen, Z. Phys. A **283**, 15 (1977).

[6] J. Eichler and S. de Barros, Phys. Rev. A **32**, 789 (1985).

[7] F. Smend and H. Czerwinski, Z. Phys. D **1**, 139 (1986).

[8] S. S. Nandi, R. Dutta, and N. Chaudhuri, J. Phys. B **20**, 4027 (1987).

[9] C. Bui and H. Milazzo, Nuovo Cimento D **11**, 655 (1989).

[10] K. M. Varier and M. P. Unnikrishnan, Nucl. Instrum. Methods Phys. Res. Sect. A **280**, 428 (1989).

[11] S. K. Ghosh, M. Ghose, S. S. Nandi, A. C. Nandi, and N. Chaudhuri, Phys. Rev. A **41**, 5869 (1990).

[12] E. Casnati, C. Baraldi, and A. Tartari, Phys. Rev. A **42**, 2627 (1990).

[13] N. G. Nayak, K. Siddappa, K. M. Balakrishna, and N. Lingappa, Phys. Rev. A **45**, 4490 (1992).

[14] L. Kissel and R. H. Pratt, Acta Crystallogr. A **46**, 170 (1990).

[15] L. Kissel and R. H. Pratt, in *Atomic Inner Shell Physics*, edited by B. Crasemann (Plenum, New York, 1985), Chap. 14.

[16] P. P. Kane, L. Kissel, R. H. Pratt, and S. C. Roy, Phys. Rep. **140**, 75 (1986).

[17] D. T. Cromer and D. A. Liberman, J. Chem. Phys. **53**, 1891 (1970).

[18] D. T. Cromer and D. A. Liberman, Acta Crystallogr. A **37**, 267 (1981).

[19] M. Deutsch and M. Hart, Phys. Rev. B **37**, 2701 (1988).

[20] C. M. Lederer and V. S. Shirley, *Table of Isotopes*, 7th ed. (Wiley, New York, 1978).

[21] J. H. Hubbell, Wm. J. Veigele, E. A. Briggs, R. T. Brown, D. T. Cromer, and R. J. Howerton, J. Phys. Chem. Ref. Data **4**, 471 (1975); **6**, 615(E) (1977).

[22] P. P. Kane, Phys. Rep. **218**, 67 (1992).

[23] M. J. Cooper, Rep. Prog. Phys. **48**, 415 (1985).

[24] E. Storm and H. I. Israel, Nucl. Data Tables A **7**, 565 (1970).

[25] P. D. Higgins, F. H. Attix, J. H. Hubbell, S. M. Seltzer, M. J. Berger, and C. H. Sibata, National Institute of Standards and Technology, Report No. NISTIR 4812, 1992.

[26] J. H. Scofield, At. Data Nucl. Data Tables **14**, 121 (1974).

[27] J. H. Scofield, Phys. Rev. A **9**, 1041 (1974).

[28] U. Bonse and G. Materlik, Z. Phys. B **24**, 189 (1976).

[29] J. C. Parker and R. H. Pratt, Phys. Rev. A **29**, 152 (1984).

[30] B. L. Henke, E. M. Gullikson, and J. C. Davis, At. Data Nucl. Data Tables **54**, 181 (1993).